Mercury emissions of a coal fired power plant in Germany

Andreas Weigelt[1,*], Franz Slemr[2], Ralf Ebinghaus[1], Nicola Pirrone[3], Johannes Bieser[1,4], Jan Bödewadt[1], Giulio Esposito[3], and Peter F.J. van Velthoven[5]

[1]Helmholtz-Zentrum Geesthacht (HZG), Institute of Coastal Research, Geesthacht, Germany

[2]Max-Planck-Institute for Chemistry (MPI-C), Department of Atmospheric Chemistry, Mainz, Germany

[3]National Research Council (CNR), Institute of Atmospheric Pollution Research, Rende, Italy

[4]Deutsches Zentrum für Luft- und Raumfahrt (DLR), Institute of Atmospheric Physics, Oberpfaffenhofen, Germany

[5]Royal Netherlands Meteorological Institute (KNMI), Chemistry and Climate Division, De Bilt, Netherlands

*now at: Federal Maritime and Hydrographic Agency (BSH), Hamburg, Germany

Correspondence to: A.Weigelt (Andreas.Weigelt@bsh.de), F. Slemr (franz.slemr@mpic.de)

andreas.weigelt@bsh.de
franz.slemr@mpic.de
ralf.ebinghaus@hzg.de
pirrone@iia.cnr.it
johannes.Bieser@hzg.de
jan.boedewadt@hzg.de
esposito@iia.cnr.it
velthove@knmi.nl

Abstract

Hg/SO_2, Hg/CO, NOx/SO_2 (NOx being the sum of NO and NO_2) emission ratios (ERs) in the plume of coal fired power plant (CFPP) Lippendorf near Leipzig in Germany were determined within the European Tropospheric Mercury Experiment (ETMEP) aircraft campaign in August 2013. The gaseous oxidized mercury (GOM) fraction of mercury emissions was also assessed. Measured Hg/SO_2 and Hg/CO ERs were, within the measurement uncertainties, consistent with the ratios calculated from annual emissions in 2013 reported by the CFPP operator, while the NOx/SO_2 ER was somewhat lower. GOM fraction of total mercury emissions, estimated by three independent methods, was below ~25%. This result is consistent with findings by others and suggests that GOM fractions of ~40% of CFPP mercury emissions in current emission inventories are overestimated.

1 Introduction

Mercury and especially methyl mercury which bio-accumulates in the aquatic nutritional chain are harmful to humans and animals (e.g. Mergler et al., 2007; Scheuhammer et al., 2007; Selin, 2009; and references therein). Therefore, Hg emissions are on the priority list of several international agreements and conventions dealing with environmental protection and human health, including the United Nations Environment Program (UNEP) Minamata convention on mercury (www.mercuryconvention.org). Mercury is emitted to the atmosphere from a variety of natural (e.g. volcanic activity, evaporation from ocean and lakes) and anthropogenic sources (e.g. coal and oil combustion) (Mason et al., 2009; Pirrone et al., 2010). Coal-fired power plants (CFPPs) are believed to account for most (≥ 56%) of mercury emitted by stationary combustion sources which constitute 35 – 77% of all anthropogenic Hg emissions (Pirrone et al, 2010; Chen et al., 2014; Ambrose et al., 2015).

Mercury from CFPPs is emitted as gaseous elemental mercury (GEM), gaseous oxidized mercury (GOM) and particulate bound mercury (PBM). Elemental mercury has a high vapour pressure, is virtually insoluble in water resulting in a long residence time in the atmosphere of about 6 - 12 months (Slemr et al., 1985; Lindberg et al., 2007; Selin, 2009; Holmes et al., 2010). GOM with its high solubility and low vapour pressure is readily washed and rained out as are the particles carrying mercury (particle bond mercury. In addition, GOM is also rapidly removed by dry deposition. GOM and PBM are believed to be in equilibrium (Rutter and Schauer, 2007; Amos et al., 2012). GOM is thus a major driver for the global mercury deposition and is estimated to make up more than 50% of the total Hg deposition (Zhang et al., 2012a; Bieser et al., 2014).

There are only two sources of GOM in the atmosphere: primary GOM emissions from anthropogenic sources and the oxidation of elemental mercury. The major anthropogenic mercury sources on a global scale are small scale artisanal gold mining (SSAG) and coal combustion (Pirrone et al. 2010). While SSAG emits solely elemental mercury, the CFPP emissions in emission inventories are estimated to have a GOM fraction between 35% and 40% (Pacyna et al., 2006; Wilson et al., 2010; EPA, 2011). However, global and regional model studies have repeatedly indicated that models are overestimating atmospheric GOM concentrations (Zhang et al., 2012b; Kos et al., 2013; Bieser et al., 2014). Possible explanations for this are an overestimation of the in-plume GEM oxidation rates or the overestimation of the amount of GOM emitted by CFPPs. The latter has been hypothesized to be due to a fast reduction of GOM inside the plume (Zhang et al., 2012b; Kos et al., 2013).

The speciation of CFPP emissions is not well known. That is because of varying composition of coal burned, complex chemistry in the stack gases (e.g. Lohman et al., 2006; Schofield, 2008; Tatum Ernest et al., 2014) and the large number of different methods used to clean CFPP flue gases with very different percentage of GOM to total mercury ranging from less than 10% up to 90% (Wang et al., 2010, Schütze et al., 2012, 2015, and references therein). Analytical problems also contribute to the uncertainty: the current emission monitoring systems are not sensitive enough to measure and speciate low mercury concentrations in flue gases of modern CFPPs (Mayer et al., 2014). Moreover, there has been evidence that the current ambient air measurement systems might not capture all oxidized mercury species with similar efficiency (Jaffe et al., 2014; Gustin et al., 2013, 2015; Weiss-Penzias et al., 2015).

The European Tropospheric Mercury Experiment (ETMEP) was carried out in July/August 2012 (ETMEP-1) and August 2013 (ETMEP-2) to measure local emissions, vertical profiles from inside the boundary layer to the lower free troposphere, and horizontal distribution of mercury over Europe. Altogether 10 measurement flights were performed over Italy, Slovenia, and Germany with two propeller aircraft. The ETMEP-1 campaign focused on volcanic emissions of Etna. The objectives of the ETMEP-2 campaign were a) to obtain vertical mercury profiles above several sites in central and southern Europe (Weigelt et al., 2016), b) to assess horizontal distribution of mercury concentrations during the flights between Italy and Germany, and c) to determine mercury emission ratios for a CFPP near Leipzig. Here, we present the measurements of CFPP emissions and their speciation.

2 Experimental

The power plant under investigation is located in Lippendorf, a small village ca. 15 km south of Leipzig in Germany. The CFPP of Lippendorf consists of two units with 934 MW gross power each. It has been in operation since 2000 and belongs with a net efficiency of 42.6% to one of the most modern and efficient lignite fuelled power plants in Europe. About 750 metric tons per hour (t/h) of lignite from a nearby open pit mine "Vereinigtes Schleenhain" are burnt together with ~ 22 t/h of sewage sludge (Schütze et al., 2015). Mercury content of lignite from two seams of "Vereinigtes Schleenhain" was 0.40 and 0.49 ppm (Rösler et al., 1977), within the range between 0.16 and 1.5 ppm for eastern German lignites (Yudovich and Ketris, 2005). No data about mercury content of the sewage sludge are available. The flue gas is directed through an electrostatic filter and a flue gas desulfurization (FGD) system to reduce particle and SO_2 emissions. The FGD is using wet washing with CaO suspension with added sulfidic precipitant and removes ~ 80% of mercury (Schütze et al., 2015). Despite the efficient FGD cleaning, the CFPP of Lippendorf ranks 4th most health harmful emitter in Germany (rating based on combined emissions of SO_2, NOx, and particulate matter, Preiss et al., 2013) and 14th most harmful emitter in Europe according to the European Environment Agency (rating based on combined emissions of SO_2, NOx, NH_3, CO_2, particulate matter, non-methane hydrocarbons, heavy metals, and organic micropollutants, EEA, 2011) with respect to health. Annual emissions reported by the operator of the CFPP Lippendorf for 2013, the year of our measurements, were: $1.18*10^{13}$ g CO_2, $1.21*10^{10}$ g SO_2, $7.91*10^{9}$ g NOx, $7.55*10^{8}$ g CO, and $4.1*10^{5}$ g Hg, among other pollutants. Mercury limit emission values (LEVs) of large combustion plants in Germany are stipulated by ordinance (Federal Law) from 2004 and its revision in 2013 to 50 µg m^{-3} as a half hour average, 30 µg m^{-3} as a daily average, and 10 µg m^{-3} as an annual average concentration (Mayer et al., 2014). Continuous monitoring of mercury emissions is mandatory but only annual total (unspeciated) mercury emissions have to be reported. European Union (EU) wide LEVs of < 5 µg m^{-3} for hard coal and < 7 µg m^{-3} for lignite fired CFPPs are under discussion (VGB, 2016).

The measurement campaign described above was performed with a CASA 212 two engine turboprop aircraft (Fig. 1a) operated by Compagnia Generale Ripreseaeree (http://www.terraitaly.it/). The CASA 212 with a maximum payload of 2.7 tons can carry the measurement instruments, different service instruments, the power supply, two pilots, and 5 operators. With a normal cruising speed of ~ 260 km h^{-1} its range is ~ 1600 km. Although the maximum flight level of the unpressurized aircraft is 8500 m, the maximum altitude of ETMEP-2 flights without oxygen supply was limited to ~3000 m above sea level (a.s.l.),

The aircraft was equipped with a gas inlet system (Fig. 1b) which had been developed and manufactured at the Helmholtz-Zentrum Geesthacht. The gas inlet was designed for the cruising speed of the CASA 212 of ~ 72 m s^{-1}. A diffuser tube reduced the air speed to ~ 5 m s^{-1}. About 120 l min^{-1} (ambient conditions) enters the inlet. The air sample is taken in the centre of the diffuser tube with a flow rate of ~ 25 l min^{-1}. The remaining flow of 95 l min^{-1} is directed to the back of the inlet where the air speed is increased by a nozzle and the air exits. By replacing the inlet and outlet nozzle with smaller or larger ones, this inlet system can be fitted to other aircraft with a different cruising speed. In the expanded area (behind the main sample line) the air temperature (T), static pressure (p), and relative humidity (rH) are measured. To avoid adsorption losses of sticky trace gases, the internal surface of the inlet system was coated with Teflon and only PFA tubing was used for the sampling lines. The outside of the inlet was coated with copper to avoid electrostatic charging. The inlet was fastened onto a 90 cm long telescope tube (6 cm diameter) which was mounted in a hole on the floor fuselage via a sliding guide. After take-off, the tube was pushed down by ~40 cm from inside the aircraft, to ensure that the inlet nozzle is outside the aircraft boundary layer. Before landing the tube was pulled back into the aircraft to protect it from damage by objects whirled up by the front wheel. The inlet and the telescope tube were equipped with heaters to prevent icing but during the ETMEP measurements the heating was always switched off because the measurement flights were carried out in summer at altitudes below 3000 m a.s.l. The tubing from the inlet to instruments (~2.5 m long 3/8’’ O.D. main sample tube with PFA manifolds to instruments) was not heated. The temperature inside the cabin was 18 to 30°C.

The aircraft was equipped with three mercury measurement instruments: a Lumex RA-915AM, a Tekran 2537B, and a Tekran 2537X (cf. Tab. 1). The Lumex RA-915 AM is based on atomic absorption spectroscopy (AAS) with Zeeman background correction (Sholupov et al., 2004) and as such measures specifically only gaseous elemental mercury (GEM) with a temporal resolution of 1 s. Its raw signal is noisy (about ± 4 ng m^{-3} with a temporal resolution of 1 s) and is dependent on pressure and temperature. Nevertheless, the fast response of the instrument is very useful to detect GEM in rather narrow highly concentrated plumes at a cruising speed of about 72 m s^{-1}. Because of thermal drifts, its zero was measured every 4 min for 1 min using an internal active carbon zero air cartridge.

The Tekran 2537B and 2537X analysers are based on preconcentration of mercury and its compounds on gold traps (Slemr et al., 1979), thermodesorption, and detection by cold vapour atomic fluorescence spectroscopy (CVAFS). Although CVAFS can detect only GEM, mercury compounds are converted to GEM during adsorption or thermodesorption (Slemr et al., 1978) and, consequently Tekran instruments can measure total gaseous mercury (TGM). The instruments use two gold traps to ensure a continuous measurement: while one is adsorbing mercury during sampling, the other one is being analysed and vice versa. The highest temporal resolution of the Tekran instruments of 150 s is given by the time necessary for the thermodesorption of mercury from the gold traps and their cooling. The Tekran 2527X analyser (Tekran 1) was run with quartz wool trap upstream of the instrument, which removes gaseous oxidized mercury (GOM) and aerosol particles with particle bound mercury (PBM) but no GEM from the air stream (Lyman and Jaffe, 2011; Ambrose et al., 2013). The Tekran 2537B (Tekran 2) analyser was operated as backup instrument without a quartz wool trap. The Teflon made (PFA and PTFE) aircraft gas inlet and tubing system are similar to the CARIBIC trace gas inlet for which high GOM transmission was qualitatively demonstrated. Based on the short residence time (0.3 sec) in the tubing to the instrument, the conditions as during an international field intercomparison (Ebinghaus et al., 1999), and higher GOM concentrations in the plume than in ambient air, we presume Tekran measurements without quartz wool trap represent total gaseous mercury (TGM = GEM + GOM). Therefore, the Tekran 2537B measurement are believed to represent TGM concentrations whereas those by Tekran 2537X GEM concentrations, both with an uncertainty of 12.5%. The uncertainty has been calculated by Weigelt et al. (2013) using two different approaches according to ISO 20988 type A6 and ISO 20988 Type A2. This uncertainty complies with the quality objective of the EU air quality directive 2004/107/EC. The instrumental setup in the aircraft was almost identical and, therefore, we expect the uncertainty to be similar.

Direct estimation of the GOM concentrations was made using three manual KCl denuder samples taken during the vertical profiles: one downwind of the Lippendorf CFPP, one upwind over the city of Leipzig (both on August 21, 2013), and one over the GMOS master site “Waldorf” in northern Germany on August 22 (Fig. 2). For sampling, the KCl denuders were connected to a bypass of the main sampling line about 1.2 m downstream the above described Teflon coated gas inlet. The sampling flow rate was controlled with a mass flow controller downstream the KCl denuder and was set to 6.4 l/min at standard temperature and pressure (STP; T=273.15 K, p=1013.25 hPa), corresponding to ~ 10 l/min at ambient temperature and pressure in 3000 m a.s.l. The sampling time was 1 hour or longer, corresponding to a total sample volume of 600 litres or more. The KCl denuder was kept at constant temperature of 50°C using a heater band. Two blank samples were also taken using KCl denuders and handled exactly in the same way as the samples (denuder preparation, installation to sampling setup, storage, analysis) but without sucking sample air through them. Five days before the ETMEP-2 campaign started all denuders were prepared for sampling by coating with KCl and were purged at 500°C for 60 min in a Tekran 1130 speciation unit with mercury free air from a Tekran active carbon zero air cartridge. During the heating mercury in the flushing air downstream the KCl denuders was measured with a Tekran 2537B mercury analyser to ensure that mercury was quantitatively removed from the KCl denuders. After the campaign the KCl denuders were analysed for their total GOM loads in the laboratory using the same setup as for the denuder preparation. The lower detection limit was estimated to be 1 pg m^{-3} and is dominated by the Tekran 2537 lower detection limit (0.1 ng m^{-3}). With about ± 5 pg m^{-3} The overall method uncertainty defined as a difference of the two blanks is with about ± 5 pg m^{-3} relatively high. Nevertheless, the method provides semi-quantitative information about GOM concentration in the plume.

We note that both methods used here to estimate GOM concentrations are subject to interferences. GOM captured by quartz wool can be released by higher air humidity (Ambrose et al., 2015) and KCl traps and denuders can release GOM in presence of high ozone and water concentrations (Lyman et al., 2010; Huang and Gustin, 2015). These interferences may result in overestimation of GEM and underestimation of GOM emissions. GEM measured by Lumex is not subject to any known interference.

For the identification and characterization of different air masses carbon monoxide (CO), ozone (O_3), sulphur dioxide (SO_2), nitrogen oxide (NO), nitrogen dioxide (NO_2), and the basic meteorological parameters temperature (T), pressure (p), and relative humidity (rH) were measured simultaneously with high temporal resolution. Instrument details including the estimated measurement uncertainty are summarised in Table 1. Uncertainties were calculated according to the individual instrument uncertainty given by the manufacturer and the calibration gas accuracy (CO, O_3, SO_2, NO). All instruments were protected from aerosols using PTFE filters (0.2 µm pore size). Model meteorological data like potential vorticity, equivalent potential temperature, relative and specific humidity, cloud cover, cloud water content, three-dimensional wind vector, as well as five day backward trajectories were calculated every 150 s along the aircraft flight tracks for additional information. These calculations are based on meteorological analysis data from the European Centre for Medium-Range Weather Forecasts (ECMWF) and the TRAJKS trajectory model (Scheele et al., 1996).

Before take-off all instruments were warmed up for at least 45 minutes, using an external ground power supply. During the starting of the engines the power was interrupted for less than 3 minutes. Since 45 minutes were too short to stabilize the Tekran 2537 internal permeation source, the Tekran instruments were calibrated only after each measurement flight before the engine shut down using the internal permeation source. All data were recalculated, using the post flight calibrations. Before and after the ETMEP-2 campaign the permeation rate of the internal permeation source was checked by manual injection of a known amount of mercury from an external mercury source (Tekran 2505 unit). During the instrument warm up, take-off and landing a Tekran active carbon zero air cartridge was inserted upstream of the Tekran instruments to prevent their contamination by the usually dirty air around airports and to enable their zeroing. All mercury instruments reported zero mercury concentration while the cartridge was inserted. The pressure in the fluorescent cells of both Tekran instruments was kept constant using upstream pressure controllers at the exits of the cells. This eliminated the known pressure dependence of the response signal (Ebinghaus and Slemr, 2000; Radke et al., 2007). The Lumex analyser has a much shorter warm up time of less than 10 minutes and was, therefore, calibrated before take-off with the internal calibration cell consisting of a sealed quartz cylinder filled with air saturated with mercury vapor. Unfortunately, the Lumex analyser does not provide the option to verify the internal calibration by injection of mercury saturated air from an external source. However, a comparison of the used Tekran- and Lumex mercury analysers before and after the ETMEP-2 campaign showed a good agreement with a difference of less than 5%. The CO instrument calibration takes 60 seconds and was, therefore, performed during the flights every 20 minutes with external calibration gas. The O_3, SO_2, NO/NO_2 instruments have a fairly constant signal response and were thus calibrated before and after the ETMEP-2 measurement campaign. Multipoint SO_2 and NO calibrations were made using dilution (Environics 300E calibrator) of certified standard gases. NO_2 conversion efficiency was determined using gas phase titration. The factory calibration was used for the pressure, temperature and relative humidity sensors. The measurements were synchronized using their individual delay and response times. Please note that all mercury (TGM, GEM, and GOM) concentrations are reported at standard temperature and pressure (STP; T = 273.15K, p = 1013.25 hPa). At these standard conditions 1 ng m^{-3} corresponds to a mixing ratio of 112 ppqv (parts per quadrillion by volume).

3 Vertical distribution and Hg/SO_2, Hg/CO, NOx/SO_2 emission ratios

The measurements were carried out on August 21 and 22, 2013. On August 21 between 9:30 and 11:20 UTC the aircraft flew many circles at different altitudes downwind of a CFPP Lippendorf (51°11`N, 12°22`E) followed between 11:25 and 12:20 UTC by a vertical profile upwind of CFPP Lippendorf over the city centre of Leipzig (51.353°N, 12.434 °E). Between 8:30 and 10:00 UTC of August 22 another vertical profile above the GMOS master site "Waldhof" (52°48`N, 10°45`E, about 200 km from Leipzig on the line connecting Leipzig and Hamburg) was flown, followed between 10:00 and 10:35 UTC by additional measurements downwind of the CFPP Lippendorf. Each vertical profile consists of at least seven horizontal flight legs, consisting of circles and altogether lasting 5 - 10 minutes each. The flight legs started inside the boundary layer at about 400 m above ground and ended at 3000 m a.s.l. The tracks of the flights on August 21 and August 22 are shown in Figure 2 and Figure 3a and 3b, respectively. The CFPP plume was encountered in the distance of ~ 7.5 km from the plant at an altitude of 1900 m a.s.l. on August 21 and in the distance of ~ 5 km at 1500 – 1650 m a.s.l. on August 22. With a wind speed of 2.4 and 1.5 m s^{-1} on August 21 and 22, respectively, the age of the plume was ~0.9 h on both days.

Figures 4 and 5 show data from the flight sections with CFPP plume encounters on August 21 and 22, 2013, respectively. The plume encounters lasted 1 – 2 min and are clearly indicated by elevated SO_2, NOx (NOx = NO + NO_2), and GEM concentrations measured by Lumex. CO and rH enhancements are hardly visible on August 21 but are clearly recognizable on August 22. Tekran instruments with a temporal resolution of 150 s are too slow to resolve individual plume encounters but they also show a broad peak of enhanced GEM (Tekran 1 with quartz wool trap) or TGM (Tekran 2) concentrations. The difference between TGM measured by Tekran without quartz wool trap and GEM measured by Tekran with quartz wool trap is small (on average 0.087 ± 0.117 ng m^{-3} (n = 8) on August 21 and 0.063 ± 0.079 ng m^{-3} (n = 12) on August 22) and varies between -0.064 and +0.354 ng m^{3} on both days. The average differences are not significantly different from zero and neither do the maximum and minimum differences exceed the combined uncertainty of the difference of 17.7%. On August 21 the plume was encountered several times at an altitude between 1600 and 2500 m a.s.l. The most pronounced encounters numbered 1 – 4 were found at an altitude of 1800 – 2250 m a.s.l. On August 22 the plume was encountered 3 times at a flight level of 1550 m and 3 times at 1650 m a.s.l. The numbered plume encounters were selected for quantitative evaluation.

Figure 6 shows the vertical distribution of the values measured downwind of the Lippendorf CFPP. The vertical profiles above Leipzig and Waldhof are discussed together with further profiles by Weigelt et al. (2016). In Figure 6 the squares represent the constant flight level measurement points (2 measurements with 2.5 minutes each). The stars represent the measurements when climbing between two flight levels (2.5 min average). The data indicated as squares are, therefore, more significant and the data illustrated as stars do provide additional information on the vertical structure. Please note that the rH, air temperature (T), and the potential temperature (θ) are plotted with high temporal resolution (1 s) in the rightmost panel. The rH can be used to distinguish between boundary layer- and free tropospheric air. Inside the planetary boundary layer (PBL) the relative humidity is usually much higher than in the free troposphere (Spencer and Braswell, 1996).

The lower four horizontal flight legs (570 to 1340 m a.s.l.) show typical northern hemispheric GEM and TGM background concentration of ~1.6 ng m^{-3} without any vertical gradient. CO, O_3, SO_2, as well as NO and NO_2 also show no vertical gradient, indicating a well-mixed PBL. This is in agreement to the other vertical profiles measured during ETMEP-2 campaign (Weigelt et al., 2016). From the fifth flight leg (1630 m a.s.l.) upward the GEM and TGM concentration increases towards the PBL top (GEM (Tekran 1): 1.7 ng m^{-3} at 1630 m a.s.l.; 2.6 ng m^{-3} at 1940 m a.s.l.; TGM (Tekran 2): 1.7 ng m^{-3} at 1630 m a.s.l.; 2.8 ng m^{-3} at 1940 m a.s.l.; GEM (Lumex): 2.1 ng m^{-3} at 1630 m a.s.l.; 2.4 ng m^{-3} at 1940 m a.s.l.). The increasing concentration is also captured by the measurements during the flight level change (GEM (Tekran 1): 1.7 ng m^{-3} at 1540 m a.s.l.; 2.1 ng m^{-3} at 1800 m a.s.l.; TGM (Tekran 2): 1.7 ng m^{-3} at 1540 m a.s.l.; 2.3 ng m^{-3} at 1800 m a.s.l.; GEM (Lumex): 1.8 ng m^{-3} at 1540 m a.s.l.; 2.2 ng m^{-3} at 1800 m a.s.l.; stars in Fig. 5). As indicated by the abrupt decrease of rH, the PBL top was found at 2150 to 2200 m a.s.l.. Consequently, the flight leg 7 at 2260 m a.s.l. and leg 8 at 3020 m a.s.l. were performed in free tropospheric air. These two measurements show a typical free tropospheric background concentration (~ 1.3 ng/m^3, Weigelt et al., 2016 and references therein). The measurements during the flight level change from leg 6 to leg 7 represent a mixture of boundary layer- and free tropospheric air (averaged altitude 2150 m a.s.l.). Therefore GEM (Tekran 1), TGM (Tekran 2), and GEM (Lumex) concentration of 2.3 ng m^{-3}, 2.4 ng m^{-3}, and 1.9 ng m^{-3} was strongly influenced by the high concentration below the boundary layer top.

In the altitude range 1600 m a.s.l. to 2200 m a.s.l. not only mercury, but also SO_2 was significantly increased (from 1.6 ppb to 21.4 ppb), which clearly indicates that the mercury was emitted from the CFPP. Inside the plume (leg 6), the O_3 concentration was slightly decreased to 42.3 ppb. At the same time NO and NO_2 increased to 6.1 ppb and 8.9 ppb, respectively. Outside the plume (e.g. leg 4) O_3 was 48.5 ppb, NO was below the detection limit, and NO_2 was ~1.5 ppb. This indicates O_3 depletion due to NO oxidation inside the plume (cf. Fig. 4 and 5). The presence of a temperature inversion at the PBL top is indicated by the changing T and θ vertical gradient in Fig. 6. This inversion layer prevents a further ascent of the power plant plume and, consequently, the highest concentration of pollutants was found below the PBL top. As already shown in Figures 4 and 5, during a flight leg in a certain altitude (and during level change) the aircraft did not remain within the plume all the time. Therefore, the concentrations, given in Fig. 6 do represent a mixture of plume and background air.

The ratio of concentration enhancements (ERs), $\Delta Hg/\Delta SO_2$, $\Delta Hg/\Delta CO$, and $\Delta NOx/\Delta SO_2$ represent the emission ratios at the stack if a) chemical reactions during the transport from the stack to the point of interception can be neglected and b) the background concentrations have not changed during the measurement including the transport from the stack to the place of plume encounters. As mentioned above, the transport time from the stack to the location of plume interception was ~ 0.9 h on both days. Based on OH concentrations measured in a CFPP plume, Ambrose et al. (2015) estimated SO_2 and NOx lifetimes of 16 – 43 and 1.8 – 5.8 h, respectively. The combination of GEM, TGM, and GOM measurements by Lumex, Tekran 2537X (Tekran 1, with quartz wool trap), 2537B (Tekran 2, without quartz wool trap), and KCl denuder, respectively, suggests that there is no substantial conversion of GEM into GOM within the transport time of ~ 0.9 h. The vertical profile over Leipzig, upwind of the CFPP, was measured on August 21 ca. 1 h after the measurements in the plume. The CO, O_3, SO_2, NOx and Hg concentrations in the PBL over Leipzig with ~ 120, 50, 0.5, 3 ppb, 1.4 ng m^{-3}, respectively, are similar to respective concentrations found outside of the plume over CFPP Lippendorf. Differences between them for SO_2, NOx, and Hg are small when compared with their enhancements in the plumes of ~ 40, 30 ppb, 4 ng m^{-3}, respectively. On August 22 no vertical profile upwind was measured, but SO_2, NOx, and Hg concentrations over Waldhof, ~ 90 km north of Leipzig, measured immediately before the downwind measurements of CFPP Lippendorf, were comparable. We thus conclude that the background concentrations of SO_2, NOx, and Hg have not changed significantly during the 0.9 h long transport from the stack to the location of aircraft interception and during ~ 20 min of the repeated plume interceptions. In addition, the large SO_2, NOx, and Hg enhancements in the plume make the calculated $\Delta Hg/\Delta SO_2$ and $\Delta NOx/\Delta SO_2$ ERs insensitive to small changes in background SO_2, NOx, and Hg concentrations. This is not always the case for small ΔCO and negative ΔO_3 (negative because O_3 is consumed by rapid oxidation of NO to NO_2) relatively to their background mixing ratios. In addition, the CO background mixing ratios changed substantially from ~123 to 105 ppb during the plume crossing #4 and #5 on August 21 due to altitude change. $\Delta Hg/\Delta CO$ for these plume interceptions was thus not calculated.

The ERs are usually calculated as a slope of Hg vs X correlations (e.g. Ambrose et al., 2015). The advantage of this method is that the background concentrations of neither Hg nor X have to be known as long as they remain constant during the measurement. The method, however, is applicable only if the plume crossings are much longer than the response time of the instruments. With the plume transects lasting in our case only 60 – 120 s and effective temporal resolution of 10 s for SO_2 and NOx measurements, however, the signals have to be carefully synchronized. In addition, the correlation slopes for individual plume crossings will become quite uncertain because of small number of points. For this reason we apply the correlation method for all (synchronized) points with SO_2 mixing ratios > 10 ppb. This selection provides 35 and 45 points for Hg vs SO_2 correlations on August 21 and 22, respectively. Individual plume crossings are not resolved by this calculation. Correlations made by the bivariate Williamson-York method (Cantrell, 2008) provide a slope and its statistical uncertainty representing ER (Hg/SO_2) and its uncertainty.

An alternative method calculates ERs as a ratio of ΔHg to ΔX where ΔHg and ΔX are signal enhancements against the background integrated over the plume crossing. This method, called here “integral method”, is applicable for measurements with instruments with different response times and we will show that it can use even Tekran measurements with a temporal resolution of 150 s, although not for individual plume crossings. Opposite to the correlation method, no exact synchronization is needed. The disadvantage, however, is that the results are sensitive to the selection of background concentrations. Figures 4 and 5 show that background Hg concentrations are especially difficult to define from the Lumex measurements. We thus use the Hg background concentrations measured by the more precise Tekran instrument. As the Lumex instrument measured only GEM, we use the background measured by Tekran instrument with quartz wool (Tekran 1). The other disadvantage of the integral method is that, opposite to the correlation method, the uncertainty of ERs is difficult to quantify. We overcome this difficulty here by averaging the ERs from individual plume crossings and taking their standard deviation as a measure of ER uncertainty.

The Hg/SO_2 ERs are listed in Table 2. The correlation and integral methods provide similar results with 5.53 ± 1.10 and 5.56 ± 1.19 µmol mol^{-1}, respectively, for August 21, and 7.38 ± 0.92 and 6.32 ± 1.52 µmol mol^{-1}, respectively for August 22. The integral method with TGM (Tekran 2) and SO_2 integrals over all plume encounters provide somewhat higher Hg/SO_2 ERs but still within the uncertainties of the correlation and integral methods. The measured Hg/SO_2 ERs are smaller than the emission ratio of 10.8 µmol mol^{-1} calculated from Hg and SO_2 annual emissions reported by the CFPP operator for 2013. They are close to 5.2 – 6.5 µmol mol^{-1} determined by Ambrose et al. (2015) for Big Brown (BBS) and Dolet Hills Stations (DHS). BBS, a 1187 MW CFPP in Texas, is fired with subbituminous coal and is equipped with activated carbon injection flue cleaning. DHS, a 721 MW CFPP in Louisiana, is fired with lignite and is equipped with wet FGD, similar to the FGD of the CFPP Lippendorf.

Hg/CO ERs are frequently used to classify the origin of different plumes (Slemr et al., 2009, 2014; Lai et al., 2011, and references therein) with ERs < 0.25 µmol mol^{-1} typical for plumes from biomass burning and ERs > 0.6 µmol mol^{-1} characteristic for plumes of urban/industrial origin. The Hg/CO ERs measured in the plume of CFPP Lippendorf are listed in Table 3. The correlation method tends to yield somewhat higher Hg/CO ERs than the integral method. Because of changing background on August 21 and changing altitude on August 22, no ERs were calculated by integral method using the Tekran measurements. As mentioned before, the high background CO mixing ratios and relatively small CO enhancement in the plume make the integral method quite sensitive to the chosen background. For this reason we believe 5.2 and 9.4 µmol mol^{-1} from correlation method for August 21 and August 22, respectively, to be more reliable. The Hg/CO emission ratio from the 2013 annual emissions reported by the operator is 7.6 µmol mol^{-1}, in reasonable agreement with our measurements. Hg/CO ERs of this magnitude have never been observed so far in the plumes detected during the CARIBIC flights (Slemr et al., 2014). This is probably because only large plumes extending over several hundreds to few thousands of km can be detected by these flights. Their Hg/CO ERs are then a mixture of Hg/CO ERs from point sources embedded in plumes from larger industrial and/or urban areas.

Simultaneous NOx and SO_2 measurements allow us to calculate also the NOx/SO_2 ERs which are listed in Table 4. The ERs from the correlations and integral methods are in good agreement with each other on both days. The NOx/SO_2 ER of 0.59 mol mol^{-1} on August 21 is almost twice as large as 0.27 mol mol^{-1} on August 22, and both ERs are substantially lower than the emission ratio of 0.91 mol mol^{-1} calculated from the NOx and SO_2 emissions reported by the CFPP operator for 2013. All these NOx/SO_2 ERs are substantially larger than ~0.08 mol mol^{-1} reported by Ambrose et al. (2015) for Big Brown CFPP in Texas and corrected for the NOx loss during the transport from the stack to the point of the plume interception.

Ozone is not emitted but the ambient O_3 is consumed by a rapid reaction with NO (O_3 + NO = NO_2 + O_2) in the plume during the transport from the stack to the point of plume interception. The O_3/NOx ERs thus do not represent emission ratios and they are negative because of O_3 consumption. If only NO were emitted the O_3/NOx ER should be -1 mol mol^{-1}. O_3/NOx ERs were not calculated for August 21 because of changing O_3 background mixing ratio. The calculated O_3/NOx ERs for August 22 are listed in Table 5. The correlation method provides a slope of -0.62 ± 0.13 mol mol^{-1} while the integral method provides an ER of -1.0 ± 0.6 mol mol^{-1}. We thus conclude that the emitted NO constitute some 60 – 100% of NOx emissions.

4 GOM emissions

As mentioned earlier, the GOM measurements made here using quartz wool traps and KCl coated denuders can be both influenced by high humidity (Huang and Gustin, 2015) and those made by KCl additionally by high O_3 concentrations (Lyman et al., 2010). Because of NO emissions, the O_3 concentrations in the CFPP plumes will be lower than in ambient air making the O_3 interference unlikely. The humidity interference would lead to an underestimation of GOM concentrations measured by KCl denuders and overestimation of GEM concentrations measured by Tekran instrument with quartz wool trap. However, specific GEM measurements are provided by Lumex, an atomic absorption instrument with Zeeman background correction, albeit with a worse precision when compared to Tekran measurements.

Table 6 lists the GOM concentrations measured by the KCl denuders during the vertical profiles over Leipzig and in the plume of CFPP Lippendorf on August 21, 2013, and over Waldhof on August 22, 2013. Taking into account the uncertainty of ± 5 pg m^{-3} there is hardly any difference between GOM concentration of 5.8 pg m^{-3} measured during the vertical profile over Leipzig and 11.4 pg m^{-3} in the plume of CFPP Lippendorf on August 21. The difference of 5.6 pg m^{-3} is distributed over the vertical profile of 3000 m. Vertical profile in Fig. 6 shows that the CFPP plume was about 450 m thick. Assuming nearly zero GOM concentrations outside of this layer, the GOM concentrations in the layer would be ~ 40 pg m^{-3}. This is roughly consistent with the differences between Tekran measurements without quartz wool trap and with it. The average difference in the plume was 87 ± 117 pg m^{-3} (n=8) on August 21 and 63 ± 79 pg m^{-3} (n=12) on August 22. Related to the average TGM enhancement (Tekran without quartz wool trap) in the plume of 0.90 ng m^{-3} on August 21 and of 1.03 ng m^{-3} on August 22, the GOM concentration would represent ~ 10% and ~ 6% of TGM emissions on August 21 and 22, respectively.

An independent assessment of the GOM emissions can be made using Hg/SO_2 ERs listed in Table 2. On August 21, the Hg/SO_2 ER of 5.5 ± 1.1 µmol mol^{-1} from correlation and 5.6 ± 1.2 µmol mol^{-1} from integral methods, both based on specific GEM measurements by Lumex, are within their uncertainties consistent with 6.6 µmol mol^{-1} derived from Tekran with quartz wool trap. On August 22, the Hg/SO_2 ER of 7.4 ± 0.9 µmol mol^{-1} from correlation method is consistent with 8.1 µmol mol^{-1} determined from Tekran data, while the 6.3 ± 1.5 µmol mol^{-1} from the integral method is somewhat lower. Consequently, Hg/SO_2 ERs from less specific measurements with quartz wool trap tend to be somewhat higher but within their combined uncertainties comparable with those derived from GEM specific Lumex measurements. A comparison of Hg/SO_2 ERs measured by Tekran without and with quartz wool trap implies GOM emissions representing 13 and 9% of TGM emissions on August 21 and 22, respectively. Taking GEM specific Lumex measurements instead of those made by Tekran with quartz wool trap would imply GOM emissions representing 27 and 24% on August 21 and 22, respectively, which we consider an upper limit.

In summary, we conclude that GOM represented less than 25 % of the TGM emitted from CFPP Lippendorf on August 21 and 22, 2013. Schütze et al. (2015) provide no numerical value but their Figure 6 shows that GOM represented ~20% of total mercury emissions of the CFPP Lippendorf at operating conditions in 2013, which is consistent with our measurements. Edgerton et al. (2006) reported GOM fraction of 13, 19, and 21% of total mercury in the plumes from CFPPs Hammond, Crist, and Bowen in the U.S. Stergašek et al. (2008) reported 4% GOM fraction for Hg emissions from CFPP with FGD in Slovenia which was fired by lignite. Wang et al. (2010) found GOM fractions of 6 - 25% of all Hg emissions from five Chinese power plants with FGD. Deeds et al. (2013) found 13% of total mercury being GOM in the plume of CFPP Nanticoke in Canada. They think that discrepancy between this and 43% GOM fraction found in stack gases is due to sampling biases. Tatum Ernest et al. (2014) support their findings using a speciation technique still in development. On the other side Landis et al. (2014) report high GOM fractions of > 86% in stack gases of the CFPP Crist and 4 – 40% conversion of GOM into GEM in the plume in 0.6 – 1.3 km distance from the stack. They attribute the difference to a reduction of GOM to GEM during the plume transport. But the reduction during the plume transport cannot resolve the difference between 86% and 20% measured by Landis et al. (2014) and Schütze et al. (2015) directly in the stack of the CFPPs Crist and Lippendorf, respectively. We note that Figure 7 of Schütze et al. (2015) shows a large day-to-day variation in mercury removal efficiency of the CFPP Lippendorf which probably also applies to the GOM removal efficiency. Part of the difference GOM in stack gases of CFPP Lippendorf and CFPP Crist can thus result from day-to-day variations in GOM removal efficiency. Putting this unresolved issue aside, low fractions of GOM emissions reported here and by others (Edgerton et al., 2006; Stergašek et al., 2008; Wang et al., 2010; Deeds et al., 2013) are in contrast to the AMAP/UNEP geospatially distributed mercury emissions dataset “2010v1” (Wilson et al., 2013), which splits the speciated mercury emissions from combustion in power plants to 50% GEM, 40% GOM, and 10% PBM. As mentioned before, the FGD in CFPP Lippendorf is made by washing of the flue gas with CaO suspension with added sulfidic precipitant and this type of FGD is known to capture most of GOM (Schütze, 2013). Although no PBM was measured in this study, 10% of mercury being emitted as PBM according to the inventory is probably also an overestimation for CFPPs with FGD (Stergašek et al., 2008; Wang et al., 2010).

5 Conclusions

Plume of the coal fired power plant (CFPP) Lippendorf near Leipzig in Germany was encountered several times on August 21 and 22, 2013. On August 21 the plume was captured at below planetary boundary layer top due to a temperature inversion layer. Hg/SO_2, Hg/CO, NOx/SO_2 ERs in the plume were determined as a slope of bivariate correlations of the species concentrations and as ratios of integrals over the individual plume crossings. The measured Hg/SO_2 and Hg/CO ERs were, within the measurement uncertainties, consistent with the ERs calculated from annual emissions reported by the CFPP operator for 2013, the NOx/SO_2 ER was somewhat lower.

GOM fraction of total mercury emissions was estimated a) using GOM measurements by KCl denuders, b) from a difference between Hg measurements by Tekran instruments without and with quartz wool trap, and c) from a difference between Hg measurements by a Tekran instrument without quartz wool trap and GEM specific measurements by Lumex instrument. Despite large uncertainties in all these estimates we conclude that GOM emissions represent less than 25% of the total mercury emissions. This result is consistent with 20% found by Schütze et al. (2015) in stack gases of CFPP Lippendorf in 2013 and findings by others (Edgerton et al., 2006; Stergašek et al., 2008; Wang et al, 2010; Deeds et al., 2013). It suggests that GOM fractions of ~40% of CFPP mercury emissions in current emission inventories are overestimated. Although PBM was not measured by us, its inventoried fraction of 10% is according to the above references too high too for CFPPs with FGD.

Acknowledgements

Measurements were carried out as part of the European Tropospheric Mercury Experiment (ETMEP) within the Global Mercury Observation System project (GMOS; www.gmos.eu). GMOS is financially supported by the European Union within the seventh framework programme (FP-7, Project ENV.2010.4.1.3-2). Special thanks are due to Compagnia Generale Ripreseaeree (http://www.terraitaly.it/) in Parma/Italy and the pilots Oscar Gaibazzi and Dario Sassi for carrying out the measurement flights.

References

AMAP/UNEP, 2013: AMAP/UNEP geospatially distributed mercury emissions dataset 2010v1, available online: http://www.amap.no/mercury-emissions/datasets (20.11.2013)

Ambrose, J.L., Lyman, S.N., Huang, J., Gustin, M.S., and Jaffe, D.A.: Fast time resolution oxidized mercury measurements during the Reno Atmospheric Mercury Intercomparison Experiment (RAMIX), Environ. Sci. Technol., 47, 7285-7294, 2013.

Ambrose, J.L., Gratz, L.E., Jaffe, D.A., Campos, T., Flocke, F.M., Knapp, D.J., Stechman, D.M., Stell, M., Weinheimer, A., Cantrell, C., and Mauldin, R.L.: Mercury emission ratios from coal-fired power plants in the southeastern U.S. during NOMADSS, Environ. Sci. Technol., 49, 10389-10397, 2015.

Amos, H.M., Jacob, D.J., Holmes, C.D., Fisher, J.A., Wang, Q., Yantosca, R.M., Corbitt, E.S., Galarneau, E., Rutter, A.P., Gustin, M.S., Steffen A., Schauer, J.J., Graydon, J.A., Louis, V.L.St., Talbot, R.W., Edgerton, E.S., Zhang, Y., and Sunderland, E.M.: Gas-particle partitioning of atmospheric Hg(II) and its effect on global mercury deposition, Atmos. Chem. Phys., 12, 591-603, doi:10.5194/acp-12-591-2012, 2012.

Bieser, J., DeSimone, F., Gencarelli, C., Geyer, B., Hedgecock, I.M., Matthias, V., Travnikov, O., and Weigelt, A.: A diagnostic evaluation of modelled mercury wet depositions in Europe using atmospheric speciated high resolution observations, Environ. Sci. Pollut. Res., 21, 9995-10012,, doi:10.1007/s11356-014-2863-2, 2014.

Cantrell, C.A.: Technical note: Review of methods for linear least-squares fitting of data and application to atmospheric chemistry problems, Atmos. Chem. Phys., 8, 5477-5487, 2008.

Chen, Y., Wang, R., Shen, H., Li, W., Chen, H., Huang, Y., Zhang, Y., Chen, Y., Su. S., Lin, N., Liu, J., Li, B., Wang, X., Coveney Jr., R.M., and Tao, S.: Global mercury emissions from combustion in light of international fuel trading, Environ. Sci. Technol., 48, 1727-1735, 2014.

Deeds, D.A., Banic, C.M., Lu, J., and Daggupaty, S.: Mercury speciation in a coal-fired power plant plume: An aircraft-based study of emissions from the 3640 MW Nanticoke Generating Station, Ontario, Canada, J. Geophys. Res., 118, 4919-4935, 2013.

Ebinghaus, R., Jennings, S.G., Schroeder, W.H., Berg, T., Donaghy, T., Guentzel, J., Kenny, C., Kock, H.H., Kvietkus, K., Landing, T., Mühleck, T., Munthe, J., Prestbo, E.M., Schneeberger, D., Slemr, F., Sommar, J., Urba, A., Wallschläger, D., and Xiao, Z.:

International field intercomparison measurements of atmospheric mercury species at Mace Head, Ireland, Atmos. Environ., 33, 3063-3073, 1999..

Ebinghaus, R. and Slemr, F.: Aircraft measurements of atmospheric mercury over southern and eastern Germany, Atmos. Environ., 34, 895–903, doi:10.1016/S1352-2310(99)00347-7, 2000.

Edgerton, E.S., Hartsell, B.E., and Jansen, J.J.: Mercury speciation in coal-fired power plant plumes observed at three surface sites in the southeastern U.S., Environ. Sci. Technol., 40, 4563-4570, 2006.

EEA (European Environmental Agency): Revealing the Costs of Air Pollution from Industrial Facilities, Technical Report 15/2011, doi:10.2800/84800, Kopenhagen, 2011.

EPA (Environmental Protection Agency): Electric Generating Utility Mercury Speciation Profiles for the Clean Air Mercury Rule, EPA-454/R-11-010, November 2011. Available online: https://www3.epa.gov/ttn/chief/emch/speciation/EGU_Hg_speciation_summary_CAMR.pdf

Gustin, M.S., Huang, J., Miller, M.B., Peterson, C., Jaffe, D.A., Ambrose, J., Finley, B.D., Lyman, S.N., Call, K., Talbot, R., Feddersen, D., Mao, H., and Lindberg, S.E.: Do we understand what the mercury speciation instruments are actually measuring? Results of RAMIX, Environ. Sci. Technol., 47, 7295-7306, 2013.

Gustin, M.S., Amos, H.M., Huang, J., Miller, M.B., and Heidekorn, K.: Measuring and modelling mercury in the atmosphere: a critical review, Atmos. Chem. Phys. 15, 5697-5713, 2015.

Holmes, C.D., Jacob, D.J., Corbitt, E.S., Mao, J., Yang, X., Talbot, R., and Slemr, F.: Global atmospheric model for mercury including oxidation by bromine atoms, Atmos. Chem. Phys., 10, 12037-12057, 2010.

Huang, J., and Gustin, M.S.: Uncertainties of gaseous oxidized mercury measurements using KCl-coated denuders, cation-exchange membranes, and nylon membranes: Humidity influences, Environ. Sci. Technol., 49, 6102-6108, doi:10.1021/acs.est.5b00098, 2015.

Jaffe, D.A., Lyman, S., Amos, H.M., Gustin, M.S., Huang, J., Selin, N.E., Levin, L., ter Schure, A., Mason, R.P., Talbot, R., Rutter, A., Finley, B., Laeglé, L., Shah, V., McClure, C., Ambrose, J., Gratz, L., Lindberg, S., Weiss-Penzias, P., Sheu, G.-R., Feddersen, D., Horvat, M., Dastoor, A., Hynes, A.J., Mao, H., Jonke, J.E., Slemr, F., Fisher, J.A., Ebinghaus, R., Zhang, Y., and Edwards, G.: Progress on understanding atmospheric mercury hampered by uncertain measurements, Environ. Sci. Technol., 48, 7204-7206, doi:10.1021/es5026432, 2014.

Kaiser, R., and Gottschalk, G.: *Elementare Tests zur Beurteilung von Meßdaten*, Hochschultaschenbücher, Band 774, Bibliographisches Institut, Mannheim, 1972.

Kos, G., Ryzhkov, A., Dastoor, A., Narayan, J., Steffen, A., Ariya, P.A., and Zhang, L.: Evaluation of discrepancy between measured and modelled oxidized mercury species, Atmos. Chem. Phys., 13, 4839-4863, doi:10.5194/acp-13-4839-2013, 2013.

Lai, S.C., Baker, A.K., Schuck, T.J., Slemr, F., Brenninkmeijer, C.A.M., van Velthoven, P., Oram, D.E., Zahn, A., and Ziereis, H.: Characterization and source regions of 51 high-CO events observed during the Civil Aircraft for the Regular Investigation of the atmosphere Based on the Instrument Container (CARIBIC) flights between South China and the Philippines, 2005-2008, J. Geophys. Res., 116, D20308, doi:10.1029/2011JD016375, 2011.

Landis, M.S., Ryan, J.V., ter Schure, A.F.H., and Laudal, D.: Behavior of mercury emissions from a commercial coal-fired power plant: The relationship between stack speciation and near-field plume measurements, Environ Sci. Technol., 48, 13540-13548, 2014.

Lindberg, S., Bullock, R., Ebinghaus, R., Engstrom, D., Feng, X., Fitzgerald, W., Pirrone, N., Prestbo, E. and Seigneur, C.: A synthesis of progress and uncertainties in attributing the sources of mercury in deposition, AMBIO, 36, 19–33, 2007.

Lohman, K., Seigneur, C., Edgerton, E., and Janssen, J.: Modeling mercury in power plant plumes, Environ, Sci. Technol, 40, 3848-3854, 2006.

Lyman, S.N., Jaffe, D.A., and Gustin, D.S.: Release of mercury halides from KCl denuders in the presence of ozone, Atmos. Chem. Phys., 10, 8197-8204, doi:10.5194/acp-10-8197-2010, 2010.

Lyman, S.N., and Jaffe, D.A.: Formation and fate of oxidized mercury in the upper troposphere and lower stratosphere, Nature Geosci., 5, 114-117, doi:10.1038/NGEO1353, 2012.

Mason, R.P.: Mercury emissions from natural processes and their importance in the global mercury cycle, in *Mercury Fate and Transport in the Global Atmosphere*, eds. Pirrone, N., and Mason, R., Springer Dordrecht, 2009, pp. 173-191.

Mayer, J., Hopf, S., van Dijen, F., and Baldini, A.: Measurement of low mercury concentrations in flue gases of combustion plants, VGB PowerTech Journal, 3/2014, 64-68, 2014.

Mergler, D., Anderson, H.A., Chan, L.H.N., Mahaffey, K.R., Murray, M., Sakamoto, M., and Stern, A.H.: Methylmercury exposure and health effects in humans: A worldwide concern, Ambio, 36, 3-11, 2007.

Pacyna, E. G., Pacyna, J. M., Steenhuisen, F., and Wilson, S.: Global anthropogenic mercury emission inventory for 2000, Atmos. Environ., 40, 4048 – 4063, 2006.

Pirrone, N., Cinnirella, S., Feng, X., Finkelman, R. B., Friedli, H. R., Leaner, J., Mason, R., Mukherjee, A. B., Stracher, G. B., Streets, D. G. and Telmer, K.: Global mercury emissions to the atmosphere from anthropogenic and natural sources, Atmos. Chem. Phys., 10, 5951–5964, doi:10.5194/acp-10-5951-2010, 2010.

Preiss, P., Roos, J., and Friedrich, R.: *Assessment of Health Impacts of Coal Fired Power Stations in Germany*, report by the Institute for Energy Economics and Rational Use of Energy (IER), University of Stuttgart, March 29th, 2013.

Radke, L. F., Friedli, H. R. and Heikes, B. G.: Atmospheric mercury over the NE Pacific during spring 2002: Gradients, residence time, upper troposphere lower stratosphere loss, and long-range transport, J. Geophys. Res., 112(D19), 1–17, doi:10.1029/2005JD005828, 2007.

Rösler, H.J., Beuge, P., Schrön, W., Hahne, K., and Bräutigam, S.: Die anorganischen Komponenten der Braunkohlen und ihre Bedeutung für die Braunkohlenerkundung, Freiburger Forschungshefte, C331, 53-70, 1977.

Rutter, A.P., and Schauer, J.J.: The effect of temperature on the gas-particle partitioning of reactive mercury in atmospheric aerosols, Atmos. Environ., 41, 8647-8657, 2007.

Scheele, M. P., Siegmund, P. C. and van Velthoven, P. F. J.: Sensitivity of trajectories to data resolution and its dependence on the starting point: In or outside a tropopause fold, Meteorol. Appl., 3(3), 267–273, doi:10.1002/met.5060030308, 2007.

Scheuhammer, A.M., Meyer, M.W., Sandheinrich, M.B., and Murray, M.W.: Effects of environmental methylmercury on the health of wild birds, mammals, and fish, Ambio, 36, 12-18, 2007.

Schofield, K.: Fuel-mercury combustion emissions: An important heterogeneous mechanism and an overall review of its implications, Environ. Sci. Technol., 42, 9014-9030, doi:10.1021/es801440g, 2008.

Schütze, J., Kunth, D., Weissbach S., and Koeser, H.: Mercury vapor pressure of flue gas desulfurization scrubber suspensions: Effects of pH level, gypsum, and iron, Environ. Sci. Technol., 46, 3008-3012, doi:10.1021/es203605h, 2012.

Schütze, J.: *Quecksilberabscheidung in der nassen Rauchgasentschwefelung von Kohlekraftwerken*, Beiträge zum Umweltschutz, Band 6/2013, Shaker Verlag, Aachen, 2013.

Schütze, J., Schilling, U., Hilbert, L., Strauß, J.H., and Hörtinger, T.: Quecksilberabscheidung am Beispiel des Kraftwerks Lippendorf, VGB Power Tech, 81-87, 2015.

Selin, N. E.: Global biogeochemical cycling of mercury: A review, Ann. Rev. Environ. Resour., 34, 43–63, doi:10.1146/annurev.environ.051308.084314, 2009.

Sholupov, S., Pogarev, S., Ryzhov, V., Mashyanov, N., and Stroganov, A.: Zeeman atomic absorption spectrometer RA-915+ for direct determination of mercury in air and complex matrix samples, Fuel Process. Technol., 85, 473-485, 2004.

Slemr, F., Seiler, W., and Schuster, G.: Quecksilber in der Troposphere, Ber. Bunsenges. Phys. Chem., 82, 1142-1146, 1978.

Slemr, F., Seiler, W., Eberling, C., and Roggendorf, P.: The determination of total gaseous mercury in air at background levels, Anal. Chim. Acta., 110, 35-47, 1979.

Slemr, F., Schuster, G., and Seiler, W: Distribution, speciation, and budget of atmospheric mercury, J. Atmos. Chem., 3, 407-434, 1985.

Slemr, F., Ebinghaus, R., Brenninkmeijer, C.A.M., Hermann, M., Kock, H.H., Martinsson, B.G., Schuck, T., Sprung, D., van Velthoven, P., Zahn, A., and Ziereis, H.: Gaseous mercury distribution in the upper troposphere and lower stratosphere observed onboard the CARIBIC passenger aircraft, Atmos. Chem. Phys , 9, 1957-1969, 2009.

Slemr, F., Weigelt, A., Ebinghaus, R., Brenninkmeijer, C., Baker, A., Schuck, T., Rauthe-Schöch, A., Riede, H., Leedham, E., Hermann, M., van Velthoven, P., Oram, D., O’Sullivan, D., Dyroff, C., Zahn, A. and Ziereis, H.: Mercury plumes in the global upper troposphere observed during flights with the CARIBIC observatory from May 2005 until June 2013, Atmosphere (Basel)., 5(2), 342–369, doi:10.3390/atmos5020342, 2014.

Spencer, R. W. and Braswell, W. D.: How dry is the tropical free troposphere？Implications for global warming theory, Bull. Am. Meteorol. Soc., 78, 1097–1106, doi:10.1175/1520-0477(1997)078<1097:HDITTF>2.0.CO;2, 1996.

Stergašek, A., Horvat, M., Kotnik, J., Tratnik, J., Frkal, P., Kocman, D., Jaćimović, R., Fajon, V., Ponikvar, M., Hrastel, I., Lenart, J., Debeljak, B., and Čujež, M.: The role of flue gas desulphurisation in mercury speciation and distribution in a lignite burning power plant, Fuel, 87, 3504-3512, 2008.

Tatum Ernest, C., Donohue, D., Bauer, D., Ter Schure, A., and Hynes, A.J.: Programmable thermal dissociation of reactive gaseous mercury, a potential approach to chemical speciation: Results from a field study, Atmosphere, 5, 575-596, doi:10.3390/atmos5030575, 2014.

VBG: VGB Initiative "Hg^{cap}": Further reduction of mercury emissions from coal-fired power plants, Position paper, VBG, Essen, March 2016.

Wang, S.X., Zhang, L., Li, G.H., Wu, Y., Hao, J.M., Pirrone, M., Sprovieri, F., and Ancora, M.P.: Mercury emission and speciation of coal-fired power plants in China, Atmos. Chem. Phys., 10, 1183-1192, 2010.

Weigelt, A., Temme, C., Bieber, E., Schwerin, A., Schuetze, M., Ebinghaus, R. and Kock, H. H.: Measurements of atmospheric mercury species at a German rural background site from 2009 to 2011 – methods and results, Environ. Chem., 10(2), 102–110, doi:10.1071/EN12107, 2013.

Weigelt, A., Ebinghaus, R., Pirrone, N., Bieser, J., Bödewadt, J., Esposito, G., Slemr, F., van Velthoven, P.F.J., Zahn, A., and Ziereis, H.: Tropospheric mercury vertical profiles between 500 and 10000 m in central Europe, Atmos. Chem. Phys., 16, 4135-4146, 2016.

Weiss-Penzias, P., Amos, H.M., Selin, N.E., Gustin, M.S., Jaffe, D.A., Obrist, D., Sheu, G.-R., and Giang, A.: Use of a global model to understand speciated atmospheric mercury observations at five high-elevation sites, Atmos. Chem. Phys., 15, 2225-2225, doi:10.5194/acp-15-2225-2015, 2015.

Wilson, S., Munthe, J., Sundseth, K., Kindbom, K., Maxson, P., Pacyna, J., and Steenhuisen, F.: *Updating Historical Global Inventories of Anthropogenic Mercury Emissions to Air*. Arctic Monitoring and Assessment Programme (AMAP) Technical Report No. 3., AMAP Secretariat, Oslo; Norway, 2010.

Wilson, S., Kindborn, K., Yaramenka, K., Steenhuisen, F., Telmer, K., and Munthe, J.: Global emission of mercury to the atmosphere, in AMAP/UNEP, *Technical Background Report for the Global Mercury Assessment*, Arctic Monitoring and Assessment Programme, Oslo, Norway/UNEP Chemicals Branch, Geneva, Switzerland, 2013.

Yudovich, Y.E., and Ketris, M.P.: Mercury in coal – a review: Part 1: Geochemistry, Int. J. Coal Geology, 62, 107-134, 2005.

Zhang, L., Blanchard, P., Gay, D.A., Presbo, E.M., Risch, M.R., Johnson, D., Narayan, J., Zsolway, R., Holsen, T.M., Miller, E.K., Castro, M.S., Graydon, J.A., St. Louis, V.L., and Dalziel, J.: Estimation of speciated and total mercury dry deposition at monitoring locations in eastern and central North America, Atmos. Chem. Phys., 12, 4327-4340, 2012a.

Zhang Y., Jaegle L., van Donkelaar A., Martin R.V., Holmes C.D., Amos, H.M., Wang, Q., Talbot, R., Artz, R., Brooks, S., Luke, W., Holsen, T.M., Felton, D., Miller, E.K., Perry, K.D., Schmeltz, D., Steffen, A., Tordon, R., Weiss-Penzias, P., and Zsolway, R.: Nested-grid simulation of mercury over North America, Atmos. Chem. Phys., 12, 6095-6111, doi:10.5194/acp-12-6095-2012, 2012b.

Tables

Table 1: List of instruments in the CASA 212 research aircraft. The acronyms are: GEM = gaseous elemental mercury; GOM = gaseous oxidized mercury.

Parameter	Instrument name	Temporal resolution	Uncertainty	Lower detection limit
GEM	Lumex RA-915AM (modified, T-stabilised by Lumex company)	1 sec (raw signal)	±4 ng/m³ (1 s raw signal) ±1 ng/m³ (10 s average)	0.5 ng/m³ (120 s average)
GEM	Tekran: 2537X (with upstream quartz wool trap)	150 s	±12.5% of reading	0.1 ng·m^{-3}
GEM + unknown amount of GOM*	Tekran 2537B	150 s	±12.5% of reading	0.1 ng·m^{-3}
GOM	manually denuder samples	2600 to 3600 s	±5 pg·m^{-3}**	1 pg·m^{-3}
CO	Aero Laser AL5002	1 s	±3% of reading	1.5 ppb
O_3	Teledyne API 400E	10 s	±2% of reading	0.6 ppb
SO_2	Thermo: 43C Trace Level	10 s	±4% of reading	0.2 ppb
NO NO_2	Teledyne API M200AU	10 s 10 s	±10% of reading	0.05 ppb
Pressure	Sensor Technics CTE7001	1 s	±1% of reading	0 mbar
Temperature	LKM Electronic DTM5080	1 s	±0.13°C	-50°C
Relative Humidity (rH)	Vaisala HMT333	8 s	±1.0% rH (0-90% rH) ±1.7% rH (90-100% rH)	0%
GPS data (3d position, speed, heading)	POS AV	1 s	±5 m (horizontal)*** ±15 (vertical)***	---

* The aircraft inlet system transmission efficiency for GOM was not tested because no GOM sources were available for measurements during the flight.

** Difference of the two blank tests

*** The GPS accuracy is dependent on the number of satellites. The given numbers are estimated values.

Table 2: Hg/SO_2 enhancement ratios (ERs). Correlation method: 10 s average Hg concentrations measured by Lumex correlated with 10 s average SO_2 mixing ratios, only Hg values with SO_2 concentrations > 10 ppb were taken, uncertainties set to 1 ng m^{-3} for Lumex and 0.5 ppb for SO_2. Integral method: 1 s Lumex and SO_2 signals integrated over the duration of Lumex measurement, measurements of Tekran with quartz wool taken as Lumex background concentrations (i.e. 1.27 and 1.25 ng m^{-3} for August 21 and 22, respectively). SO_2 background mixing ratio was 0.83 and 0.66 ppb on August 21 and 22, respectively. Since Tekran with a temporal resolution of 150 s cannot resolve individual plume crossing, the integral of the Tekran signal encompasses the plumes 1 – 4 on August 21 and the plumes 1 – 6 on August 22.

Date	Method	Species	ER 10^{-6} mol mol^{-1}	n, R, signif	Comment
August 21, 2013	correlation	GEM	5.53 ± 1.10	35, 0.6564, >99.9%	
	integral peak 1	GEM	6.67		Lumex zeroing
	integral peak 2	GEM	5.72		
	integral peak 3	GEM	5.98		Lumex zeroing
	integral peak 4	GEM	3.88		
	integral peak 5	GEM	0.89		
	integral average	GEM	5.56 ± 1.19*	4*	
	Tekran with quartz wool trap	GEM	6.56		
	Tekran without quartz wool trap	TGM	7.55		
August 22, 2013	correlation	GEM	7.38 ± 0.92	45, 0.7751, >99.9%	
	integral peak 1	GEM	6.44		
	integral peak 2	GEM	4.83		
	integral peak 3	GEM	5.90		Lumex zeroing
	integral peak 4	GEM	6.67		
	integral peak 5	GEM	9.03		Lumex zeroing
	integral peak 6	GEM	5.02		
	integral average	GEM	6.32 ± 1.52	6	
	Tekran with quartz wool trap	GEM	8.13		
	Tekran without quartz wool trap	TGM	8.97		
2013	reported annual emissions	TGM	10.8		

*average without integral of peak 5 which is identified as outlier by Nalimov test (at >95% significance level, Kaiser and Gottschalk, 1972)

Table 3: Hg/CO enhancement ratios (ERs). Correlation method: 10 s average Hg concentrations measured by Lumex correlated with 10 s average CO mixing ratios for SO_2 mixing ratios above 10 ppb, uncertainties set to 1 ng m^{-3} for Lumex and 1 ppb for CO. Integral method: 1 s Lumex and CO signals integrated over the duration of Lumex measurement, readings of Tekran with quartz wool taken as Lumex background concentrations (i.e. 1.27 and 1.25 ng m^{-3} for August 21 and 22, respectively). CO background mixing ratio was 119.3 ppb on August 21 and 123.8 ppb on August 22.

Date	Method	ER (Hg/CO)		Comment
		10^{-5} mol mol^{-1}	n, R, signif	
August 21, 2013	Correlation	5.19 ± 0.94	31, 0.6596, >99.9%	values only until 10:40:20
	integral peak 1	3.40		Lumex zeroing
	integral peak 2	4.16		
	integral peak 3	3.33		Lumex zeroing
	integral peak 4			background change
	integral peak 5			CO calibration
	integral average	3.63 ± 0.46	3	
August 22, 2013	Correlation	9.43 ± 1.07	37, 0.7880, >99.9%	
	integral peak 1	3.19		
	integral peak 2			CO calibration
	integral peak 3			Lumex zeroing, CO calibration
	integral peak 4	7.87		
	integral peak 5	5.61		Lumex zeroing
	integral peak 6	4.75		
	integral average	5.36 ± 1.95	4	
2013	reported annual emissions	7.58		

Table 4: NOx/SO_2 enhancement ratios (ERs). Correlation method: 10 s average NOx mixing ratios correlated with 10 s average SO_2 mixing ratios above 10 ppb, uncertainties set to 1 ppb for NOx and 0.5 ppb for SO_2. Integral method: 1 s NOx and 1 s SO_2 signals integrated over the duration of the individual plume intersection, background mixing ratios for SO_2 and NOx are 0.83 and 1.78 ppb, respectively, for August 21 and 0.66 and 0.45 ppb, respectively for August 22.

Date	Method	ER (NOx/SO_2)		Comment
		mol mol^{-1}	n, R, signif	
August 21, 2013	Correlation	0.585 ± 0.038	34, 0.9379, >99.9%	
	integral peak 1	0.598		
	integral peak 2	0.575		
	integral peak 3	0.725		
	integral peak 4	0.497		
	integral peak 5			
	integral average	0.598 ± 0.095	4	
August 22, 2013	Correlation	0.262 ± 0.051	40, 0.6344, >99.9%	
	integral peak 1	0.297		
	integral peak 2	0.457		
	integral peak 3	0.167		Lumex zeroing
	integral peak 4	0.330		
	integral peak 5	0.133		Lumex zeroing
	integral peak 6	0.317		
	integral average	0.284 ± 0.118	6	
2013	reported annual emissions	0.910		

Table 5: O_3/NOx enhancement ratios (ERs). Correlation method: 10 s average O_3 mixing ratios correlated with 10 s average SO_2 mixing ratios above 10 ppb, uncertainties set to 1 ppb for O_3 and 1 ppb for NOx. Integral method: 1 s O_3 and 1 s NOx signals integrated over the duration of the individual plume intersection, background mixing ratios for O_3 and NOx are 43.09 and 1.78 ppb, respectively, for August 21. Individual O_3 background mixing ratios (average of background before and after the peak) varying between 53.9 ppb for peak 1 to 56.2 ppb for peak 4 were taken for August 22. The NOx background mixing ratio on August 22 was 0.45 ppb.

Date	Method	ER (O_3/NOx)		Comment
		mol mol^{-1}	n, R, signif	
August 22, 2013	Correlation	-0.620 ± 0.134	40, -0.3776, >95%	
	integral peak 1	-0.979		
	integral peak 2	-0.424		
	integral peak 3	-1.527		
	integral peak 4	-0.686		
	integral peak 5	-2.059		
	integral peak 6	-0.568		
	integral average	-1.040 ± 0.633	6	

Table 6: Results of the manual KCl denuder samples during all ETMEP-2 measurement flights in 2013 over central Europe. GOM data were corrected for denuder blanks determined over Iskraba/Slovenia and Waldhof/Germany. GOM concentrations are given as a centre of an estimated uncertainty range (in brackets) and are given at standard temperature and pressure (STP; T=273.15 K, p=1013.25 hPa).

Date	**Location**	**Profile character (relative sampling time in PBL* and FT** air**	**analysed GOM concentration [pg m^{-3}]**
2013-08-21	Lippendorf/Germany	vertical (76% PBL: 24% FT)	11.4 (7.0-15.7)
2013-08-21	Leipzig/Germany	vertical (61% PBL; 39% FT)	5.8 (1.0*** - 10.6)
2013-08-22	Waldhof/Germany	vertical (54% PBL; 46% FT)	31.0 (24.6-37.3)

* planetary boundary layer (PBL)

** free troposphere (FT)

***If a concentration was found to be below the method lower detection limit of 1.0 pg m^{-3}, the lower detection limit is given.

Figures

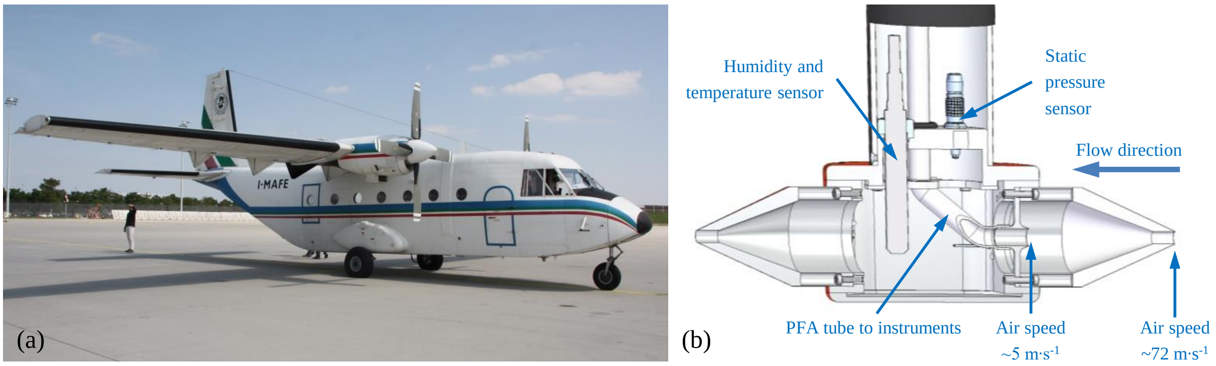

Figure 1: For the ETMEP-2 campaign in August 2013 the CASA 212 (a) from the Italian company Compagnia Generale Ripreseaeree (http://www.terraitaly.it/) was equipped with specially designed and manufactured trace gas inlet (b).

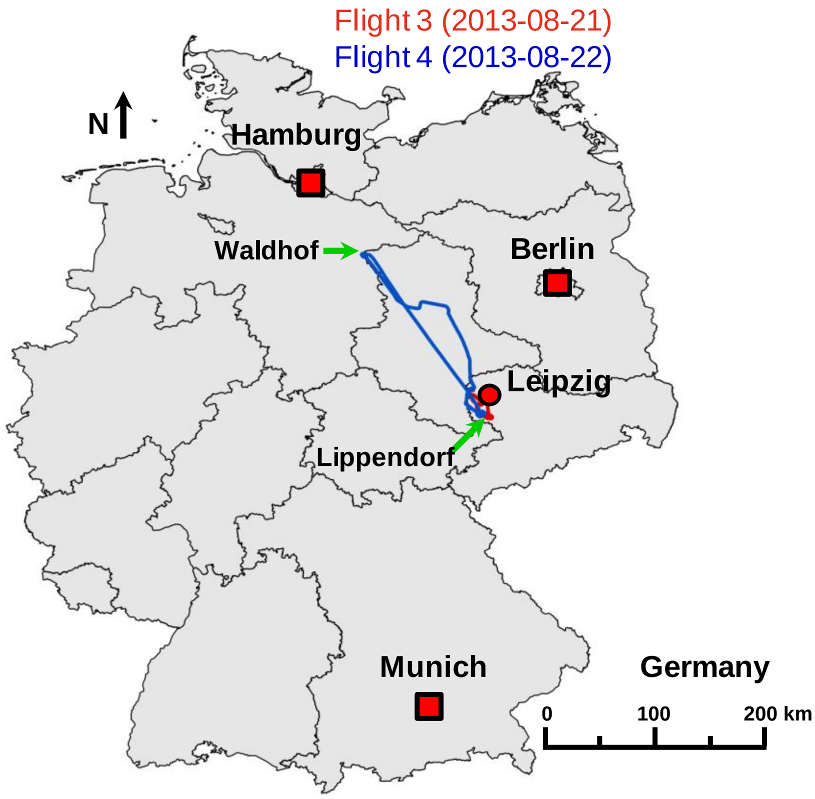

Figure 2: Flight tracks of the ETMEP-2 measurement flights number 3 and 4 over Central and northern Germany. The flights were made from the Leipzig airport.

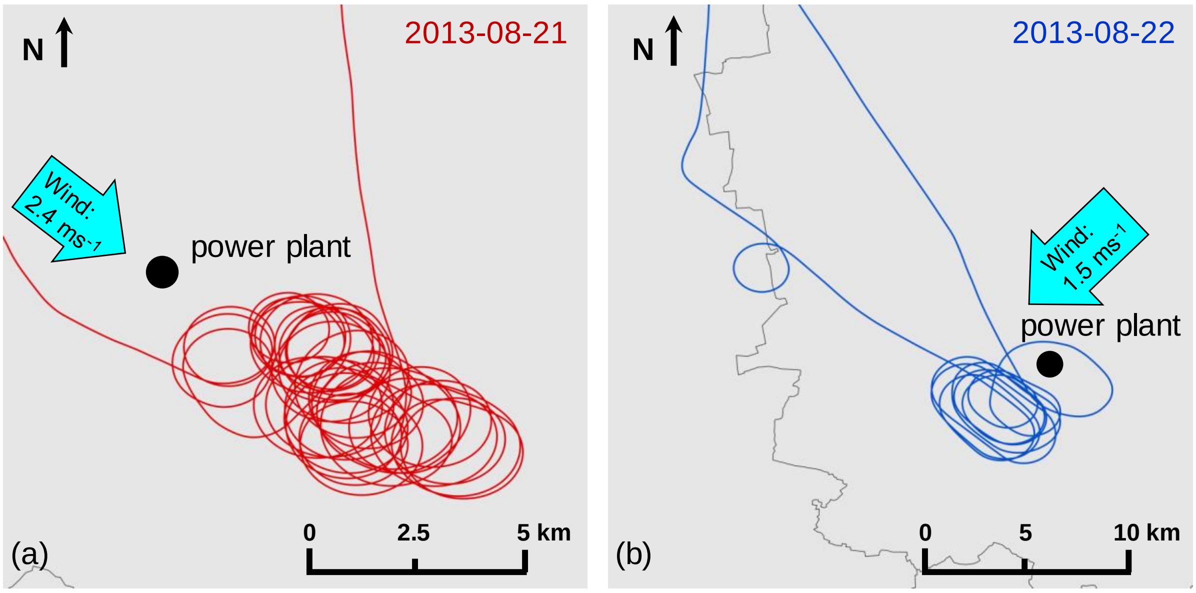

Figure 3: Flight tracks of the ETMEP-2 flights on August 21 (a) and 22 (b), 2013, downwind of the lignite fired power plant "Lippendorf", south of Leipzig, Germany. On both flights the power plant plume was crossed several times.

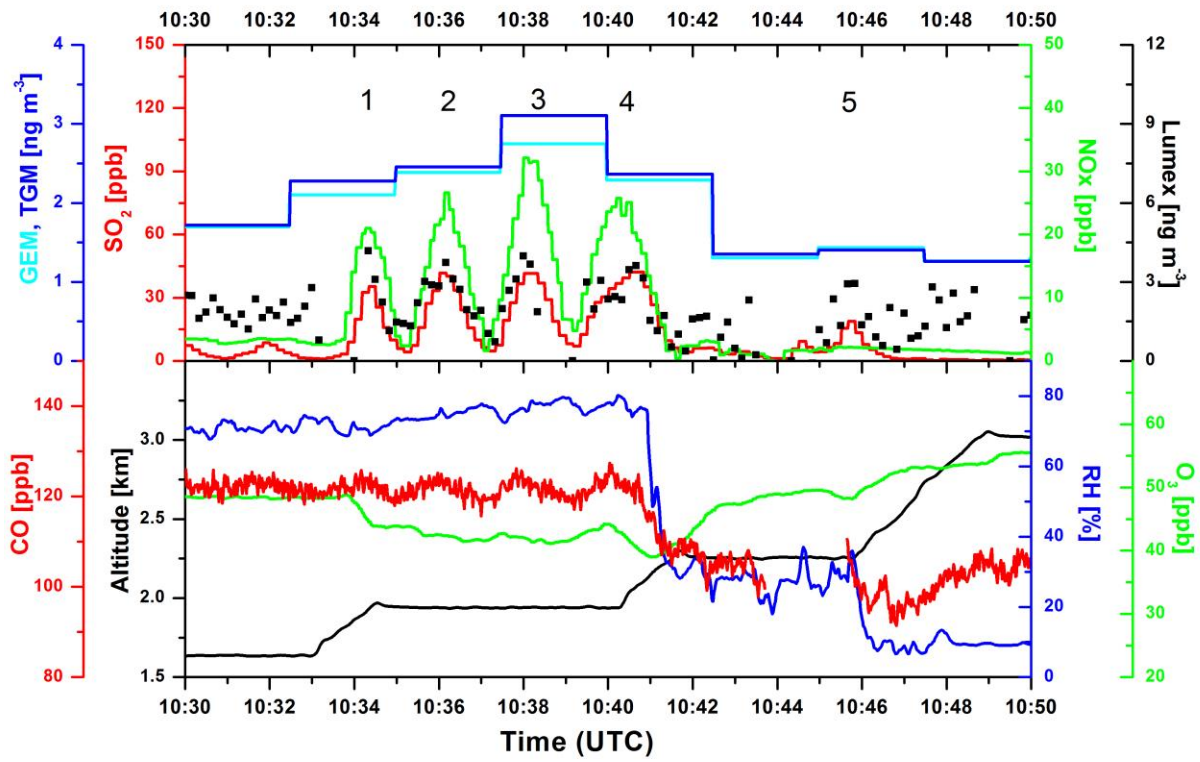

Figure 4: ETMEP-2 lignite fired power plant plume measurements on August 21, 2013 south of Leipzig/Germany. The gaps in the Lumex signal (10 s resolution) are due to internal zero air checks for the correction of the instruments base line drift. GEM was measured using Tekran instrument run with quartz wool trap at the inlet of the instrument which is presumed to remove GOM. TGM was measured by another Tekran instrument with no quartz wool trap at the inlet. All parameters were synchronized using individual instrument delay and response times. All Hg concentrations are given at standard temperature and pressure (STP; T=273.15 K, p=1013.25 hPa).

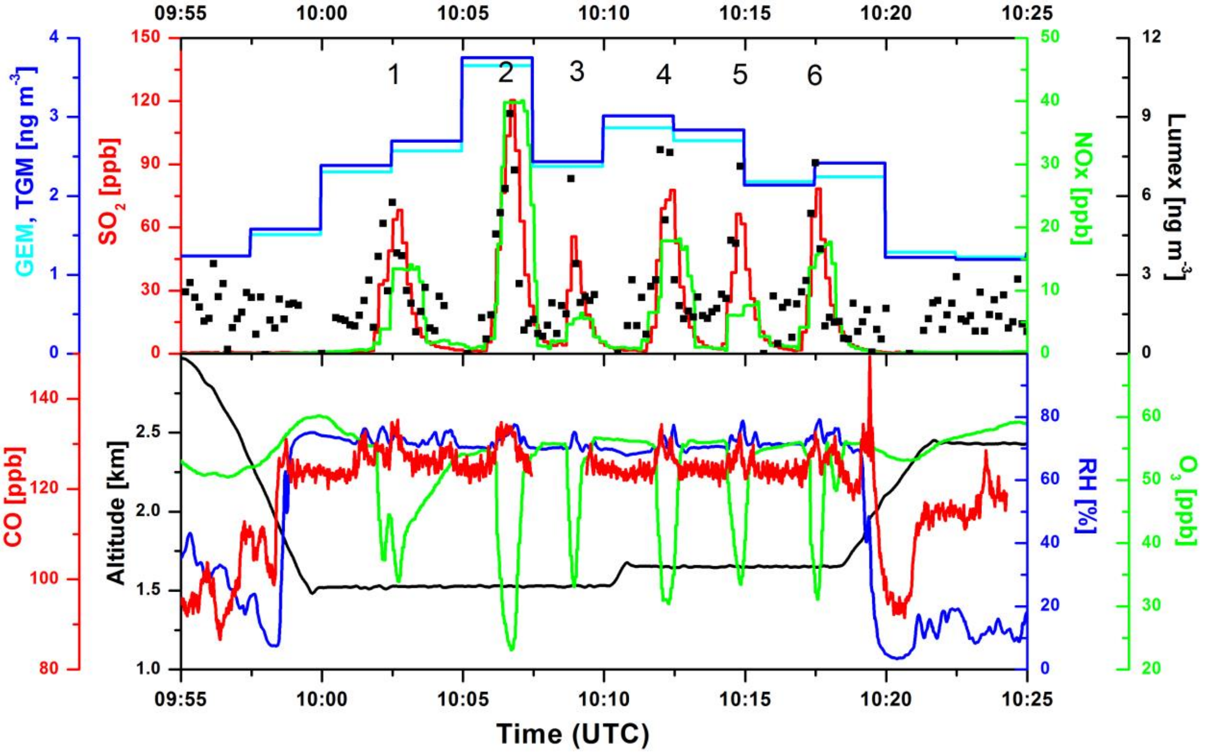

Figure 5: The same as in Figure 4, but for measurements on August 22, 2013.

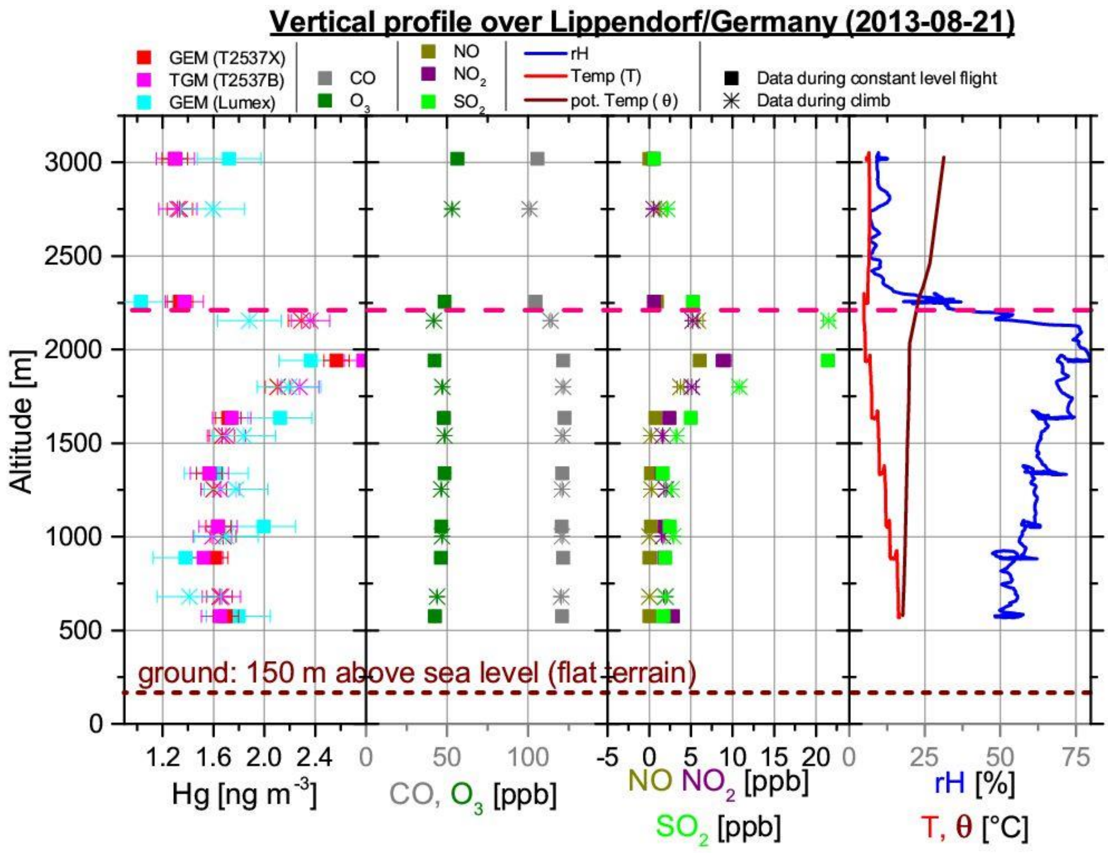

Figure 6: Vertical profile, measured on 21 August 2013 from 13:17:30 to 14:07:30 (local time) downwind the coal fired power plant Lippendorf (central Germany; 45.561°N, 14.858 °E, elevation: 150 m a.s.l.; flat terrain). Squares represent 300 s averages with horizontal flight leg; stars indicate 150 s averages during climbing between two neighbouring flight legs. The red dashed line indicates the planetary boundary layer (PBL) top, which was determined to be at 2150 to 2250m a.s.l.. All Hg concentrations are given at standard temperature and pressure (STP; T=273.15 K, p=1013.25 hPa).